A Comparison of Selected Strategies for Adaptive Control of Wave Energy Converters

Jørgen Hals[1]
e-mail: jorgen.hals@ntnu.no

Johannes Falnes

Torgeir Moan

Centre for Ships and Ocean Structures (CeSOS),
Norwegian University of Science and Technology (NTNU),
Otto Nielsens v. 10,
7491 Trondheim, Norway

Wave-energy converters of the point-absorbing type (i.e., having small extension compared with the wavelength) are promising for achieving cost reductions and design improvements because of a high power-to-volume ratio and better possibilities for mass production of components and devices as compared with larger converter units. However, their frequency response tends to be narrow banded, which means that the performance in real seas (irregular waves) will be poor unless their motion is actively controlled. Only then the invested equipment can be fully exploited, bringing down the overall energy cost. In this work various control methods for point-absorbing devices are reviewed, and a representative selection of methods is investigated by numerical simulation in irregular waves, based on an idealized example of a heaving semisubmerged sphere. Methods include velocity-proportional control, approximate complex conjugated control, approximate optimal velocity tracking, phase control by latching and clutching, and model-predictive control, all assuming a wave pressure measurement as the only external input to the controller. The methods are applied for a single-degree-of-freedom heaving buoy. Suggestions are given on how to implement the controllers, including how to tune control parameters and handle amplitude constraints. Based on simulation results, comparisons are made on absorbed power, reactive power flow, peak-to-average power ratios, and implementation complexity. Identified strengths and weaknesses of each method are highlighted and explored. It is found that overall improvements in average absorbed power of about 100–330% are achieved for the investigated controllers as compared with a control strategy with velocity-proportional machinery force. One interesting finding is the low peak-to-average ratios resulting from clutching control for wave periods about 1.5 times the resonance period and above. [DOI: 10.1115/1.4002735]

Keywords: ocean waves, renewable energy, reactive control

1 Introduction

An early result of wave energy research (see review articles by Evans [1] and Falnes [2]) was that the maximum useful absorbed energy for a body oscillating in one mode is achieved provided that the intrinsic reactance $X_i(\omega)$ is canceled and that the load resistance $R_m(\omega)$ equals the intrinsic resistance $R_i(\omega)$. (The word *intrinsic* is here used to signify the systems own impedance terms, including friction and viscous losses, but excluding machinery forces.) This corresponds to what in electric circuit theory is known as *impedance matching*.

Falnes [3] (Chap. 6) described two alternative strategies for achieving this:

1. complex conjugate control
2. phase and amplitude control

As illustrated by Fig. 1, where Z_i is the complex intrinsic impedance, the first alternative corresponds to providing a direct feedback from the velocity of the buoy. Now this represents a challenge in that the velocity-to-force transfer function $-Z_i^*(\omega)=-R_i(\omega)+iX_i(\omega)$ becomes inherently *anticausal* (i.e., transforms to a left-sided impulse response function) because of the complex conjugation. In other words, the optimal machinery force depends solely on future values of the buoy velocity, which is obviously impossible to implement in practice, as the velocity depends on our choice for the machinery force. We are thus compelled to search for realizable (sub-optimal) approximations for the practical implementation, and this will be treated here.

The other alternative, phase, and amplitude control (shown as $F_{m,2}$ in Fig. 1), is to feed forward the excitation force through a transfer function $H_v(s)=1/\{2R_i(s)\}$ yielding the optimal velocity $v^{\text{opt}}(s)=F_e(s)/\{2R_i(s)\}$ as a reference signal (where it is assumed that the radiation resistance $R_i(\omega)$ can be approximated by a rational Laplace transform function; $R(\omega)\approx R(s)|_{s=i\omega}$). A controller can then be programmed to track the desired velocity, a common application of control engineering. But this alternative is also encumbered by causality trouble; the transfer function is *noncausal* (i.e., transforms to a two-sided impulse response function [3], Sec. 6.3), but this can be overcome in an approximative manner if we are able to predict the future excitation force, or by approximating the transfer function $H_v(s)$ by a causal function. In principle, the span of information about the future wave needed for optimal control depends on the geometry of the device, while the available information depends on the coherence of the incident wave as explained by Price et al. [4].

Both of these alternatives for optimal control imply that the machinery has to handle a reactive power flow and may therefore be categorized under the broader classification of *reactive control*.

Perdigão et al. [5] reported a solution for approximating the complex conjugate control applied to an oscillating water column device. Looking at control alternatives for the Archimedes wave swing (AWS), Beirão [6] tried to apply internal model control as a means to approximate optimal velocity tracking, and achieved a

[1]Corresponding author.

Contributed by the Ocean Offshore and Arctic Engineering Division of ASME for publication in the Journal of Offshore Mechanics and Arctic Engineering. Manuscript received December 7, 2009; final manuscript received May 3, 2010; published online March 29, 2011. Assoc. Editor: Takeshi Kinoshita.

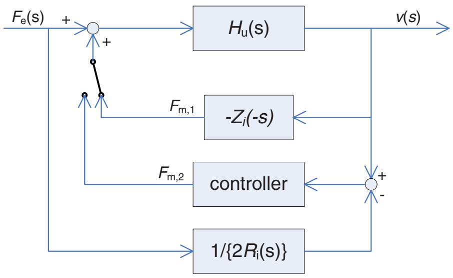

Fig. 1 Block diagram showing alternatives paths for optimal control of the wave energy converter represented by $H_u(s)$. The choice between $F_{m,1}$ and $F_{m,2}$ corresponds to the choice between complex conjugate control, and phase and amplitude control, respectively [3] (Fig. 6 and 7). We have assumed that the hydrodynamic parameters can be approximated by rational Laplace transform functions, $R(\omega)\approx R(s)|_{s=i\omega}$ and $m_r(\omega) \approx m_r(s)|_{s=i\omega}$.

reasonable performance. He also demonstrated the use of linearization feedback control applied to a nonlinear model of the AWS.

In a more recent approach Gieske [7] tried to apply model-predictive control (MPC) to wave energy conversion, also with AWS as the example. This method resembles what Eidsmoen [8] tried to do when he optimized the converter's response over a short future horizon by the use of force predictions. The application of MPC to wave energy converters was further studied by Hals et al. [9] and has shown to yield power absorption close to optimum in irregular waves.

All of approximations to optimal control described above require that the machinery handles reactive power. A set of controllers for wave energy absorbers that do not involve reactive power flow may be classified as *resistive bang-bang controllers*. *Latching* and *clutching control* belong here. These ideas derived as an intuitive way of achieving optimum oscillation phase by keeping the absorber fixed during parts of the cycle (latching) or by coupling and decoupling the machinery at intervals (clutching) [10,11]. Hoskin and Nichols [12] used a variational calculus approach and showed that latching control belongs to a class of solutions that in optimal control theory is known as bang-bang control [13], i.e., the optimal solution is for the control variable to switch between its minimum and maximum allowed values. The same goes for clutching control.

The challenge in implementing latching and clutching control strategies is twofold: (i) designing a durable mechanism or method to carry out the latching/unlatching (or coupling/decoupling in the case of clutching control) and (ii) to determine the unlatching instants. In principle, one needs to know the excitation ahead in the same manner as for the non-causal transfer function resulting from the optimality conditions referred to above. This task was already solved with promising results about 30 years ago [14,15]. For more complex systems, with more than one degree of freedom, the application of latching control has shown to be more challenging [16,17], although mathematical description inspired by Thévenin's equivalent for electrical circuits may ease the problem [18]. A simplified approach was taken by Falcão [19], who, inspired by rectifying hydraulic valves, omitted the need for prediction by introducing a threshold-triggered unlatching. This principle was verified and developed further by Lopes et al. [20].

Although very similar to latching, the clutching control idea appeared later and has received less attention in the wave energy literature. The key point is that instead of being locked, the oscillator is moving freely during parts of the oscillation cycle. The notions *freewheeling* [11] and *unlatching* [21] control have also been used for this strategy. Kamensky et al. [10] showed that for unconstrained oscillation of a harmonic oscillator, clutching can be preferable to latching in some conditions. In a recent study, Babarit et al. [22] showed that clutching is theoretically superior to strategies of pseudocontinuous control that try to mimic the behavior of, e.g., a linear damper.

Evans [23], Pizer [24], and Falnes [25] consecutively discussed the influence of global motion constraints on wave energy absorption. Their results were based on a frequency-domain approach. Evans and Pizer both presented examples on how such constraints influence the performance of a heaving sphere absorber. Recently Hals et al. [9] studied optimal constrained motion for the same kind of absorber using a time-domain method. Many devices are designed with physical end stop mechanisms such as spring and dashpot components [26] or water brakes [27].

There have been numerous suggestions on how to predict the incoming wave, both in the case of remote and local wave monitoring [4]. A standard solution for estimating and predicting signals is Kalman filtering (see, e.g., Ref. [28]). By running the filter equations iteratively based on the current filter states, a priori estimates for future values may be extrapolated. In Ref. [9] an augmented Kalman filter was used to provide useful predictions 2–4 s ahead based solely on local monitoring, and the same method will be used here.

Another question is how to tune the control parameters. The classical solution for adaptive control is *gain scheduling* (see, e.g., Ref. [29]). The parameters are then updated based on a predefined plan, which may be based on experience or on a model giving the optimal parameter settings for different operating conditions; in our case for different sea states. An old method for self-tuning regulators that has regained interest in recent years is *extremum-seeking control* [30]. It is a powerful method for real-time optimisation of the control parameter that only requires that a purposeful convex objective function may be defined, and which in general works at rates of adaptation almost as fast as the plant dynamics. Here we apply this method to maximize the power output from wave energy converters.

The purpose of this article is to study how a representative selection of the mentioned control strategies can be implemented for online control and to compare their performance and properties. We begin, in Sec. 2, by presenting our model of a heaving semisubmerged sphere, which will serve as a generic example for the wave-absorbing body, and then proceed, in Sec. 3 by defining and explaining the control algorithms and the assumptions made. Finally, the simulation scheme, results and analysis are reported in Secs. 4 and 5.

2 Converter Model

In order to keep the investigation at a generic level, a heaving semisubmerged sphere will be used as an example for the wave energy converter. Dynamics of other types of converters will have similar properties, although they can be more complex. The model used is sketched in Fig. 2 and includes the following effects:

- *Net restoring stiffness force* $F_s=\rho g A_w \eta$, which is the difference of the gravitational and buoyancy forces, where ρ is the water density, g is the acceleration of gravity, $A_w=\pi r^2$ is the water plane area, and η is the heave excursion.
- *Inertia force* $F_i=m\ddot{\eta}$ due to the mass m of the moving body with acceleration $\ddot{\eta}$.
- *Wave excitation force* F_e, which is the sum of pressure forces on the body surface due to incident and diffracted waves.
- *Wave radiation force* F_R due to the radiated wave when the body moves. It may be written as $F_R=m_\infty\ddot{\eta}+\int_0^t k(\tau)\dot{\eta}(t-\tau)d\tau$, where the retardation function $k(t)$ is related to the radiation resistance (or wave damping coefficient) R_r by $k(t)=(2/\pi)\int_0^\infty R_r(\omega)\cos(\omega t)d\omega$ [31]. The factor $m_\infty=\lim_{\omega\to\infty} m_r(\omega)$, where $m_r(\omega)$ is the added mass. The convolution term, which we will denote F_r, may be approximated by a state-space model [32,33]; $\mathbf{z}=\mathbf{A}_r\mathbf{z}+\mathbf{B}_r\dot{\eta}$, with

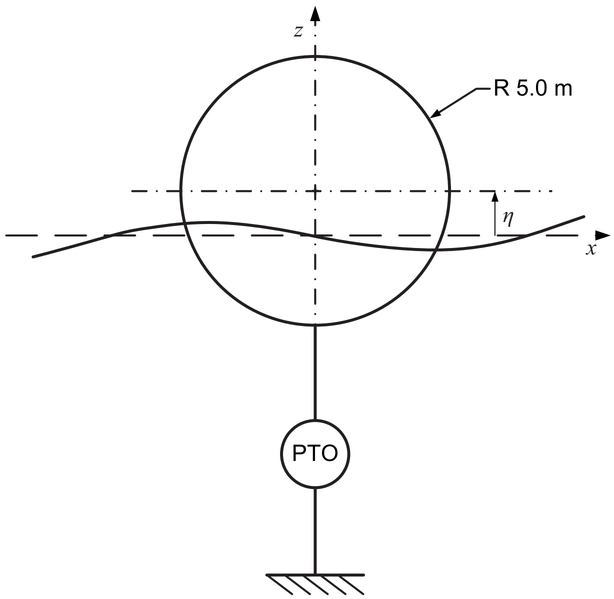

Fig. 2 An illustration of the heaving sphere used as a wave energy absorber in this work. Its radius r is 5 m and it is semisubmerged at its equilibrium position, i.e., the mass $m = \rho 2\pi r^3/3$. A power take-off system (PTO) is connected between the buoy and a fixed reference, giving a force F_m on the buoy.

output equation $F_r = \mathbf{C}_r \mathbf{z}$, where $\mathbf{z}$ is an additional state vector, and $\mathbf{A}_r$, $\mathbf{B}_r$, and $\mathbf{C}_r$ are the state, input, and output matrices, respectively.

- *Machinery force* F_m, which is the subject of this work, and which is assumed to follow the command given by the controller, i.e., it is assumed strong and fast enough to immediately follow a set-point.

The hydrodynamic forces (excitation and radiation) are approximated by linear theory, i.e., both motions and wave amplitudes are assumed to be small. The reference point against which the machinery works is assumed to be rigid, and possible dynamics of connecting wires or struts are not accounted for.

An equation of motion for the heave mode may then be given as [31]

$$F_i + F_R + F_s = F_e + F_m \tag{1}$$

or, explicitly,

$$(m + m_\infty)\ddot{\eta} + \int_0^t k(\tau)\dot{\eta}(t-\tau)d\tau + \rho g A_w \eta = F_e + F_m \tag{2}$$

With a state-space approximation for the convolution term as mentioned above, the whole model may be rewritten in state-space form as

$$\dot{\mathbf{x}}(t) = \begin{bmatrix} 0 & \dfrac{-\rho g A_w}{1+m_\infty/m} & \dfrac{-\mathbf{C}_r}{1+m_\infty/m} \\ 1/m & 0 & 0_{1\times 4} \\ \mathbf{B}_r/m & 0_{4\times 1} & \mathbf{A}_r \end{bmatrix} \mathbf{x}(t) + \begin{bmatrix} \dfrac{1}{1+m_\infty/m} \\ 0 \\ 0_{4\times 1} \end{bmatrix} (F_m(t) + F_e(t)) \equiv \mathbf{A}\mathbf{x}(t) + \mathbf{B}(F_m(t) + F_e(t)) \tag{3}$$

Here $x_1 = m\dot{\eta}$, $x_2 = \eta$, and $[x_3, \ldots, x_N]^{\mathrm{T}} = \mathbf{z}$, where N-2 is the order of the state-space approximation for the convolution term F_r. For the heaving sphere, a model of order four has shown to be sufficient for F_r. The total model thus consists of six first-order ordinary differential equations and may be solved by conventional tools for numerical integration. In block diagrams to be shown later, the model is represented by the system transfer function

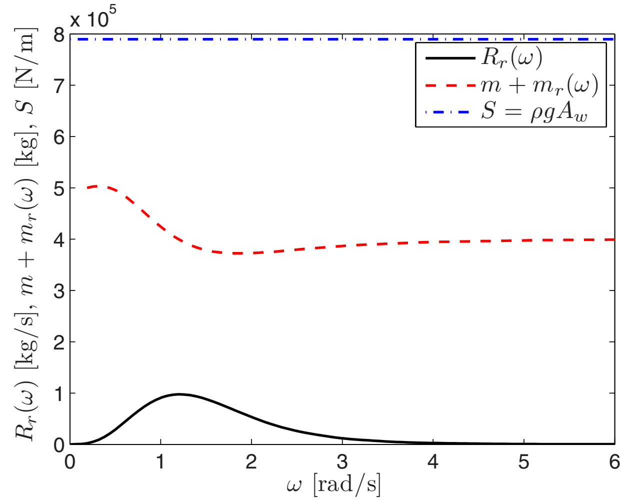

Fig. 3 Hydrodynamic parameters for a semi-submerged heaving sphere of radius 5 m. The radiation resistance $R_r(\omega)$ is given by the black curve, the red dashed curve gives the sum of physical mass and added mass $m + m_r(\omega)$, and the hydrostatic stiffness S, which is approximated by a constant, is shown by the blue dash-dotted curve.

$H_u(s) = (s\mathbf{I} - \mathbf{A})^{-1}\mathbf{B}$, giving the system states as output.

In the following, we will need the notion of intrinsic resistance R_i and reactance X_i [3] (p. 184). These are frequency dependent (in a manner governed by the body mass and geometry), and their functions for the heaving sphere are shown in Fig. 3. In our case we have assumed that there is no viscous or frictional loss, so the intrinsic resistance $R_i(\omega)$ is equal to the radiation resistance $R_r(\omega)$, which is due to outgoing waves. The reactance depends on the added mass $m_r(\omega)$ and the buoyancy stiffness $S = \rho g A_w$ for heave motion, and is defined by $X_i(\omega) = \omega(m + m_r(\omega)) - S/\omega$.

The hydrodynamic parameters are shown in Figs. 3 and 4.

3 Control Methods

In this section, the various control algorithms considered in this study and their implementation are described and discussed. The question asked is how to control the machinery force F_m.

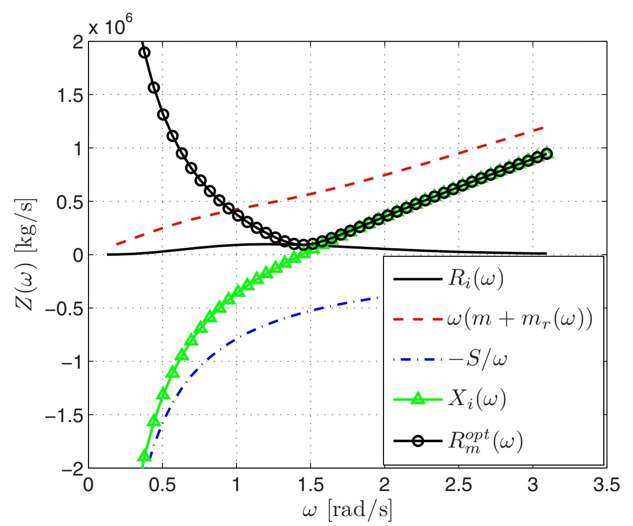

Fig. 4 Intrinsic impedance terms for the heaving sphere. Also shown is the optimal load resistance $R_m^{\mathrm{opt}} = \sqrt{R_i(\omega)^2 + X_i(\omega)^2}$ for nonreactive control.

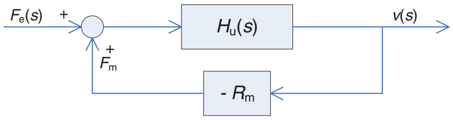

Fig. 5 Block diagram for the RL strategy. It gives a machinery force directly proportional to the buoy velocity $v(s)$. The dynamics of the heaving buoy is represented by the transfer function $H_u(s)$.

3.1 Resistive Loading (RL). A very common assumption within wave energy modeling has been to assume the following form for the machinery force:

$$F_m(t) = -R_m \dot{\eta}(t), \tag{4}$$

such that the machinery force depends linearly on the velocity $\dot{\eta}$, with a resistance R_m as coefficient of proportionality. The strategy defined by Eq. (4) may be given as the block diagram shown in Fig. 5. We include it here for reference and because it is often used as a useful starting point in modeling and simulation studies as well as laboratory experiments and prototyping. Time series of force, position, and velocity signals for this strategy are shown in Fig. 6.

With such a machinery force, the optimal setting for the load resistance is known to be $R_m^{\mathrm{opt}}(\omega)=\sqrt{R_i^2(\omega)+X_i^2(\omega)}$, where R_i and X_i are the intrinsic resistance and reactance, respectively [34].

It may be seen from Fig. 4 that the further we are from resonance, the larger the optimal R_m^{opt} term will be. This lowers the response amplitude but reduces the phase difference between force and velocity (cf. phase and amplitude control). As the resulting machinery force is proportional to the velocity there is no reactive power flow, and with the requirement $R_m > 0$, the machinery never has to work in motor mode. For irregular waves, we explore a simplified approach by choosing a constant R_m, different for each sea state.

3.2 Approximate Complex-Conjugate Control (ACC). With impedance matching, the optimal control force may be written $F_m^{\mathrm{opt}}(\omega)=-Z_m^{\mathrm{opt}}(\omega)u(\omega)=-Z_i^*(\omega)u(\omega)$, i.e., the optimal machinery impedance Z_m^{opt} equals the complex conjugate of the intrinsic impedance $Z_i(\omega)=R_i(\omega)+iX_i(\omega)$ [35,3]. (The minus sign occurs because of the way we have defined the machinery force, see Eq. (1).) As discussed in Sec. 1, we then need to find a causal approximation $Z_m(s)|_{s=i\omega}$ to the optimal feedback function $Z_m^{\mathrm{opt}}(\omega)$ giving a system as illustrated in Fig. 7.

For a monochromatic wave input of angular frequency ω_k, this optimal force may be written as the time-domain function

$$F_m^{\mathrm{opt}}(t) = (m + m_r(\omega_k))\,\ddot{\eta}(t) - R_i(\omega_k)\,\dot{\eta}(t) + S\,\eta(t) \tag{5}$$

Keeping the same function with constant coefficients (from a properly chosen ω_k) for operation in irregular waves could serve as a simple approximation. We must, however, be careful in order

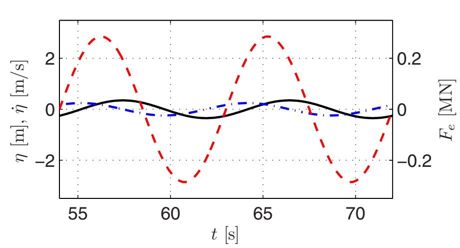

Fig. 6 Regular wave (T=9 s and H=1 m) time series example for the RL strategy. The red dashed curve gives the excitation force F_e, the blue dash-dotted curve gives the velocity $v=\dot{\eta}$, and the fully drawn black curve gives the heave position η.

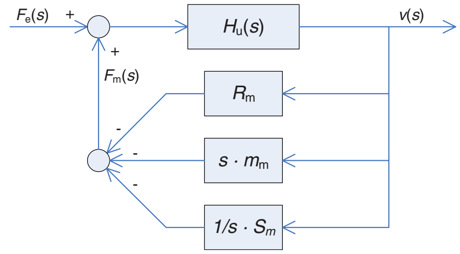

Fig. 7 Block diagram for the ACC control. The machinery force is the sum of terms proportional to position, velocity and acceleration.

to ensure that the controlled system becomes stable.

Let us now simplify the WEC model (3) by replacing the frequency-dependent parameters m_r and R_i by constants so that we get

$$\dot{\mathbf{x}}(t) = \begin{bmatrix} -R_c/m_c & -S \\ 1/m_c & 0 \end{bmatrix}\mathbf{x}(t) + \begin{bmatrix} 1 \\ 0 \end{bmatrix}(F_m(t) + F_e(t)) \tag{6}$$

with $x_1=m_c\dot{\eta}$. Using the velocity variable $v(s)=\mathcal{L}\{\dot{\eta}(t)\}$, Eq. (6) has the Laplace-plane equivalent

$$m_c s v(s) + R_c v(s) + S\frac{v(s)}{s} = F_e(s) + F_m(s) \tag{7}$$

In this case, the intrinsic impedance is

$$Z_i(s) = m_c s + R_c + \frac{1}{s}S = \frac{m_c s^2 + R_c s + S}{s} \tag{8}$$

and the machinery impedance may be written as

$$Z_m(s) = \frac{m_m s^2 + R_m s + S_m}{s} \tag{9}$$

with optimal values $m_m=-m_c$, $R_m=R_c$, and $S_m=-S$ according to the complex conjugate relation behind Eq. (5). The machinery force is now

$$F_m(s) \equiv -Z_m(s)v(s) = -\frac{m_m s^2 + R_m s + S_m}{s}v(s) \tag{10}$$

By cancellation of m_c and S terms, this gives the optimal response velocity

$$v(s) = \frac{F_e(s)}{2R_c} \tag{11}$$

as it should. The force-to-velocity transfer function of the total controlled system becomes

$$H_{v,F_e} = \frac{1}{Z_i(s)+Z_m(s)} = \frac{1}{(m_c - m_m)s^2 + (R_c + R_m)s + (S - S_m)} \tag{12}$$

Now to the point: We see that if m_m and S_m are larger than the intrinsic values m_c and S, the coefficients become negative (giving positive poles) and the controlled system will be unstable. Using this as a simplification for the wave energy converter, we may place the poles of the controller such that we are sure not to get positive poles. It can be done by looking at the minimum values for $m+m_r(\omega)$ and S and choosing the controller parameters m_m and S_m with some safety margin, see Fig. 3. We see that stability may be ensured by choosing constant values $m_m \le 3.72\times10^5$ kg and $S_m \le 7.90\times10^5$ N/m. (We have used the values 3.5×10^5 kg and 7.5×10^5 N/m, respectively.) The parameter R_m may be taken as a parameter to be optimized for each sea state. Figure 8 shows a time series example for the ACC strategy.

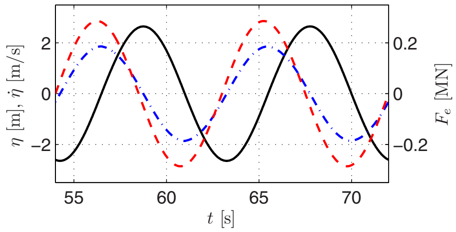

Fig. 8 Regular wave (T=9 s and H=1 m) time series example for the ACC strategy. Line patterns as in Fig. 6.

3.3 Tracking of Approximate Optimal Velocity (AVT). As mentioned in Sec. 1, the phase and amplitude control yield an expression for the optimal velocity and may therefore be seen as a velocity tracking problem. The question is how to approximate the optimal velocity function $v^{\mathrm{opt}}(\omega)=F_e/\{2R_i(\omega)\}$. Here we will simply replace $R_i(\omega)$ by a constant R_c so that $v_{\mathrm{ref}}=F_e/\{2R_c\}$, and we will see how the choice of its value influences the result. We have not tried to find a frequency dependent approximation to $1/\{2R_i(\omega)\}$ although it could be worthwhile investigating, for instance, as described in Ref. [5] and also in Ref. [3] (Sec. 6.3).

Once having defined the reference signal, the tracking can be done with a simple P or PI controller. Thus the whole scheme can be pictured as in Fig. 9, with

$$Z_{\mathrm{PI}}(s) = \beta K_{\mathrm{P}} \frac{1 + T_i s}{1 + \beta T_i s} \tag{13}$$

We have used $K_{\mathrm{P}}=5\times 10^7$ Ns/m, $\beta=1.2$, and $T_i=4.2$ s. A time series example for operation in regular waves is shown in Fig. 10.

3.4 Model-Predictive Control (MPC). The application of model-predictive control to this problem was studied in a recent work [9], and we only outline the principles here. The idea is to optimize the expected response of the system over a short future horizon T_h using a discrete time model of the conversion unit together with a prediction of the input force. The maximization of power output under the chosen constraints may be cast into a quadratic programming (QP) optimization problem, which guarantees that a solution is found. By moving the time window of predictions along as the time is running, the optimization may be solved anew at predefined intervals, finding the best control force

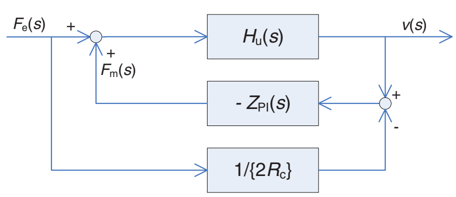

Fig. 9 Block diagram for the approximate optimal velocity tracking (AVT) strategy. The velocity reference signal is tracked by the use of a PI controller $Z_{PI}(s)$.

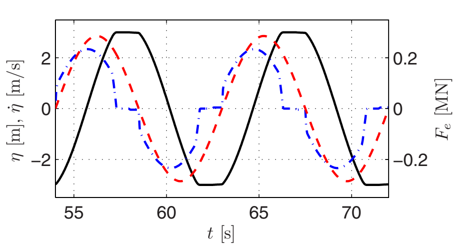

Fig. 10 Regular wave (T=9 s and H=1 m) time series example for the AVT strategy. Line patterns as in Fig. 6.

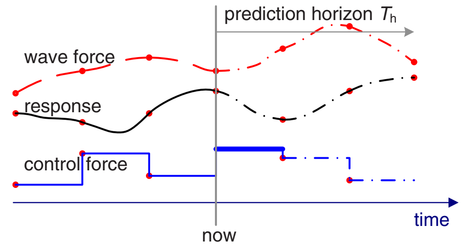

Fig. 11 The moving prediction horizon principle of model-predictive control (MPC). The control force is changed in discrete time steps that are short compared with the system dynamics (i.e., in practice shorter than shown here). At each discrete time step a new optimization of the predicted response is calculated using the predicted excitation force as input, and the first element of the machinery force vector is applied to the system (indicated by the thick line).

at each instant given the instantaneous states and conditions. The scheme is illustrated by Figs. 11 and 12. A time series example of MPC is shown in Fig. 13.

The MPC controller fully exploits our knowledge about the system (including constraints) and is therefore able to provide a control that is close to constrained optimal.

3.5 Phase Control by Latching (PML and TUL). Latching control is achieved by halting the motion each time the velocity becomes zero, and releases it according to a certain rule such that the phase between velocity and excitation force is improved compared with the passive (RL) case. For regular waves the unlatching rule may be defined as fixed intervals of latching, but in irregular waves this does not work well because the time interval between force maxima varies. A fruitful strategy is to aim at aligning the peaks of the force and velocity signals [36,37], and this may be approximately achieved by releasing the buoy approximately $T_0/4$ before the next (predicted) peak for the wave force ($T_0\approx 4.4$ s being resonance period). Here we denote this strategy by *peak-matching latching control*, abbreviated PML, and a block

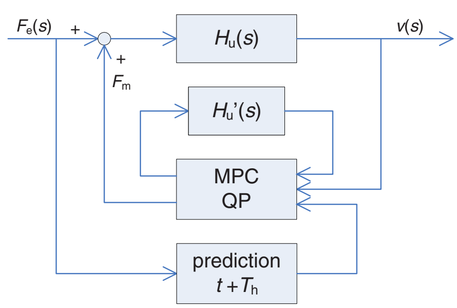

Fig. 12 Block diagram for the MPC strategy. A QP optimization problem is solved at each discrete time step of the controller. The prediction horizon is set to span an interval over which the force prediction is reasonably accurate. Here T_h=2.2 s have been used.

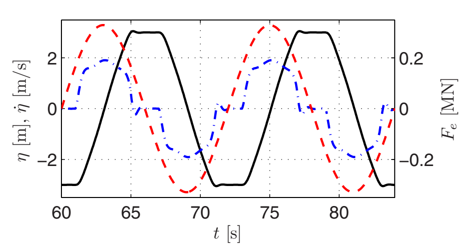

Fig. 13 Regular wave (T=9 s and H=1 m) time series example for the MPC strategy. Line patterns as in Fig. 6.

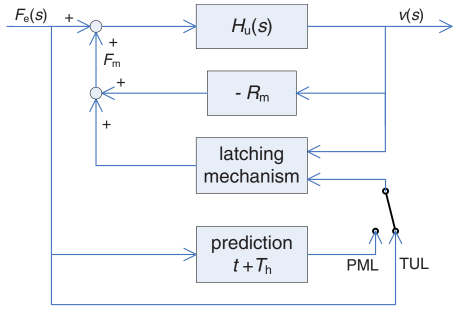

Fig. 14 Block diagram for the PML and TUL control strategies. The latching mechanism is used to hold the buoy in a fixed position. During motion the machinery force is proportional to the buoy velocity.

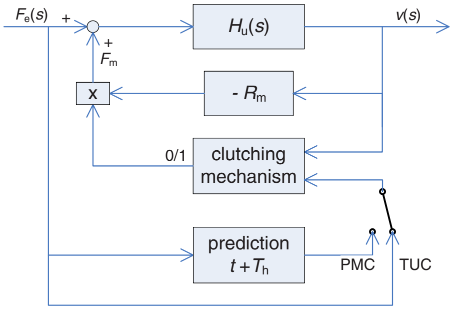

Fig. 16 Block diagram for the PMC and TUC control strategies. The clutching mechanism is used to engage and disengage the machinery force. When engaged, the machinery force is proportional to the buoy velocity.

diagram for the controller is shown in Fig. 14. The time series example follows in Fig. 15.

Instead of aligning peaks, Falcão [19] and Lopes et al. [20] suggested a method that does not rely on predicted values for the excitation, but rather only on an estimation of the instantaneous excitation force. The principle tells that the buoy should be released once the force passes a chosen threshold, thus we will refer to it as threshold unlatching control (TUL). In regular waves the result is identical to PML, but in irregular waves there will be differences in the unlatching instants. Obviously, either strategy is best suited for incident waves of typical period $T > T_0$. Luckily, at least for heaving point absorbers, the physics of the problem tells that this will most often be the case. (It should be mentioned that Babarit et al. [37] showed that latching may also be useful for the case where $T < T_0$.)

During the unlatched intervals the machinery load resistance, R_m, is kept constant at a value that may be optimized for each sea state. In real-world designs the latching may be achieved by clamping brakes, hydraulic control valves or other. For modeling and simulation purposes, two alternative methods have been common. The first method is to have two models for the system: one for the latched state ($v=0$) and one for the moving state ($v = f(F_e(t), R_m, t)$), and to switch between these at the right instants. The other is to introduce an additional large resistance R_l in the mathematical model, which is active during latching intervals and zero otherwise. Thus here no assumption is made about how the latching mechanism is realized, although the latter method may be seen as a simple model of a clamping brake. The two methods give practically no difference in the result as long as the resistance is chosen large enough. We use the second approach with $R_l \geq 1 \times 10^9$ kg/s. Because the power take-off is only resistive, the latching control machinery has no reactive power flow.

3.6 Phase Control by Clutching (PMC and TUC). The only difference between clutching and latching is that the resistance is switched between zero and a constant instead of between a (different) constant and a very large value (in principle infinite). This results in time series of the kind shown in Fig. 17, and a block diagram is given in Fig. 16. Although very similar, there are, as we shall see, some important differences in the performance of latching and clutching controllers. With clutching control, the power is harvested during a slow sliding motion from the outer positions (see Fig. 17), whereas with latching it is harvested during the transitions between outer steady positions (see Fig. 15).

3.7 Parameter Tuning. The MPC controller optimizes the control input to the system on a wave-to-wave time scale. Because of this it can lead to a performance close to what is the theoretical optimum. All the controllers defined above have a structure where parameters need to be tuned on a longer time scale, say from a duration corresponding to wave-group or sea state variation. Here we will consider the adaptive schemes referenced in the introduction, namely, gain scheduling and extremum-seeking control.

3.7.1 Gain Scheduling. If we disregard end stop interference, most of the controller parameters depend on the wave frequency only (once the device geometry has been set). A good approximation to the optimal parameter settings is then achieved by using knowledge about the average wave period. All that is needed is then an online estimate of the instantaneous average period, and the parameters may be set according to a predefined schedule. If the relation between wave frequency and parameter settings is not known, the schedule may be established based on experience or trial and error. For the threshold unlatching and unclutching strategies, information about the wave heights are also needed [20].

In our implementation, we have processed the last 100 zero up-crossing periods in computing the needed statistical measures.

3.7.2 Extremum Seeking. Extremum seeking control is a powerful method for real-time optimization where a modulation of the control input is used to drive the control parameters to their optimum value. The method does not depend on having a model of the process; all that is needed is that the control goal can be formulated as an objective function that is convex in the control parameters. It may be freely defined by the control designer. The

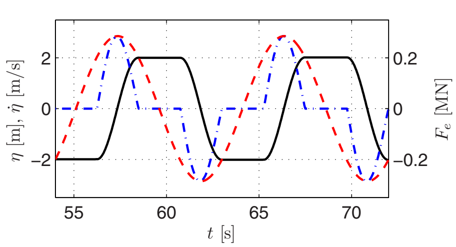

Fig. 15 Regular wave (T=9 s and H=1 m) time series example for the PML and TUL strategies. Line patterns as in Fig. 6.

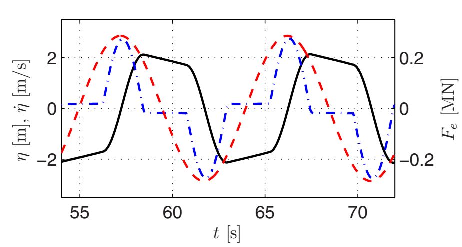

Fig. 17 Regular wave (T=9 s and H=1 m) time series example for the PMC and TUC strategies. Line patterns as in Fig. 6.

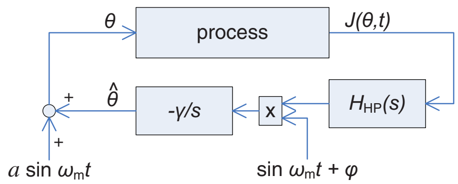

Fig. 18 Block diagram for the extremum-seeking control algorithm. A modulation signal $a\sin(\omega_m t)$ is added to the parameter setting $\hat{\theta}$. The objective function J is chosen as the output from the process, and it is high-pass filtered (H_{HP}) to retain only value changes. The multiplication serves as a demodulation, and the result is low-pass filtered by the $-\gamma/s$ block [38,30].

scheme is illustrated by Fig. 18.

The crucial point in order to succeed with extremum-seeking design is thus the definition of the objective function. For the application to wave energy we wish to maximize the average converted power and therefore need to filter out the power variation due to the zero-crossings of velocity (which gives instants of zero power conversion). And we wish for a measure that represents the absorbed useful power, but which is quite constant even though the incident wave power level is changing. On this background, we have defined the objective function J as an approximation to the absorption width by low-pass filtering the useful power $P_u(t)=F_m(t)v(t)$ and dividing by the low-pass filtered squared excitation force:

$$J(t)=\frac{h_{\mathrm{LP}}(t)\star P_u(t)}{h_{\mathrm{LP}}(t)\star F_e(t)^2} \tag{14}$$

where $h_{\mathrm{LP}}(t)$ is the low-pass filter, and $\star$ signifies convolution. A second-order low-pass filter $H(s)=1/(1+Ts)^2$ with $T=57.3$ s has been used here.

3.8 Constraint Handling/State Saturation. In the same way as physical end stops may be introduced in order to restrict the stroke of moving bodies, virtual end stops may be incorporated in the controller in order to avoid that the bodies reach the physical end stops, or to reduce the impact when limits are reached. Control methods for handling this kind of state saturation is common in motion planning for robots, where obstacles may be represented by repulsive potentials (see, e.g., [39], Chap. 5]). For the problem at hand, a corresponding effect may be achieved by adding spring and/or damper terms to the calculation of the machinery force set-point, for instance,

$$F_m=R_m\dot{\eta}-\mathrm{sign}(\eta)S_{\mathrm{es}}(|\eta|-\eta_{\mathrm{lim}})u(|\eta|-\eta_{\mathrm{lim}})-R_{\mathrm{es}}\dot{\eta}u(|\eta|-\eta_{\mathrm{lim}}) \tag{15}$$

where $u(\cdot)$ is the Heaviside step function, and S_{es} and R_{es} are the spring and damping constants for the end stop mechanism. The constant η_{lim} gives the excursion for which the mechanism starts acting. Once included in the simulation model, the added force terms may be seen as either representing a physical end stop, or as a part of the control force. In the calculation of power output we have in this paper done the former, i.e., the power dissipated due to the additional terms are not included in the numbers for useful absorbed energy.

For the velocity tracking control (AVT), it is, however, better to modify the reference signal in order to avoid conflict with the PI controller. It can be done by requiring that the velocity never exceeds a value corresponding to oscillation at a chosen frequency $\omega_{\max}$ and with amplitude equal to the stroke limit $\eta_{\max}$. This is illustrated by Fig. 19. In mathematical terms, this may be written as

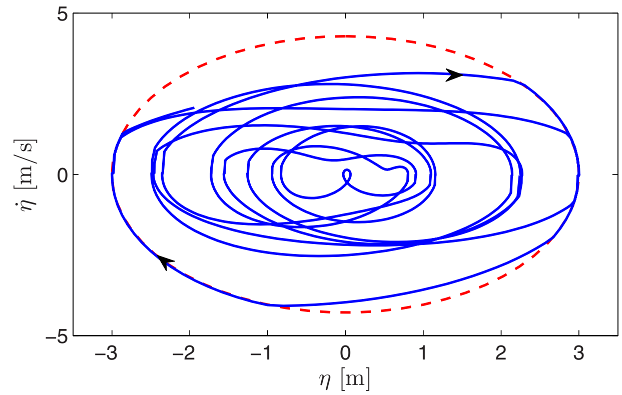

Fig. 19 Phase plot showing the amplitude constraints principle for velocity tracking control. The red dashed line gives a saturation limit for the combined state of position η and velocity $\dot{\eta}$.

$$v_{\max}=\begin{cases}0 & \text{for} \quad (|\eta|>\eta_{\max})\wedge(v_{\mathrm{ref}}\eta>0)\\ \omega_{\max}\sqrt{\eta_{\max}^2-\eta^2} & \text{otherwise}\end{cases} \tag{16}$$

We thus modify the velocity reference v_{ref} according to

$$v'_{\mathrm{ref}}=\mathrm{sign}(v_{\mathrm{ref}})\max(|v_{\mathrm{ref}}|,v_{\max}) \tag{17}$$

This principle has similarities with *sliding-mode control* [40], although the goal is not to drive the state to a chosen reference, but rather to ensure that it stays within the given state limits.

This method is also a fruitful alternative to the virtual end stop (Eq. (15)) for the other controllers (except MPC). By modifying the machinery force with a term that is proportional to the deviation from the limiting velocity/position characteristics, one can get a smoother behavior of the virtual end stop; for instance, by adding a term

$$F_v=-R_v(|\dot{\eta}|-v_{\max})u(|\dot{\eta}|-v_{\max})\mathrm{sign}(\dot{\eta}) \tag{18}$$

to the machinery force of Eq. (15) to get $F'_m=F_m+F_v$. This has been tested and gives a smoother impact with the end stop, which can be adjusted by the parameter $\omega_{\max}$, but it has not been used for the results to be presented in Sec. 5.

4 Simulation Set-Up

The example model (Sec. 2) has been simulated with the controllers defined in Sec. 3 for a range of regular and irregular waves. The mathematical model (3) and the controllers were implemented in MATLAB/SIMULINK [41], and the hydrodynamic parameters and excitation force coefficients were calculated by WAMIT [42]. A range of regular and irregular waves was then defined based on wave period T and wave height H. For irregular waves, the energy period T_e and significant wave height H_s were used as parameters and nine different sea states were synthesized from a Bretschneider spectrum, see Table 1. The irregular wave time series have length equal to about 160 times the energy period of the sea state. Exactly the same time series were used for all runs with the same sea state parameters. In the calculation of average and

Table 1 Wave power level J (kW/m) for the irregular wave sea states studied

H_s (m)	T_e (s) 6.0	9.0	12.0
4.24	53.0	79.5	106
2.83	23.5	35.3	47.1
1.41	5.89	8.83	11.8

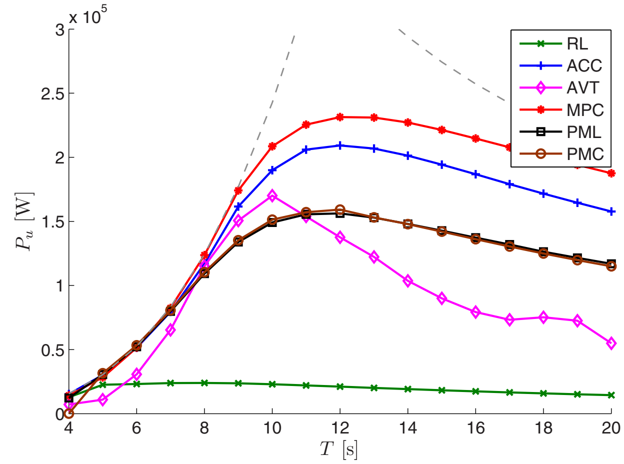

Fig. 20 Budal diagram showing the average absorbed power for the different control strategies with varying wave period of regular waves with height H=1 m

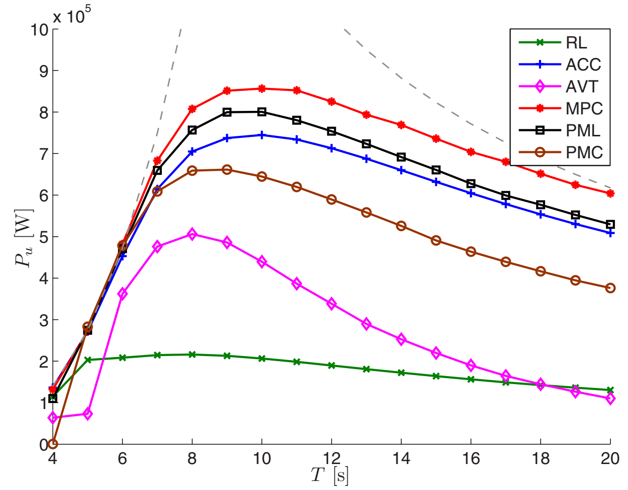

Fig. 21 Budal diagram showing the average absorbed power for the different control strategies with varying wave period. The incident waves were regular with height H=3 m.

peak values, short intervals of about five average wave periods at the beginning and on average wave period at end of the time series were excluded in order to avoid transient and end-point effects.

Due to the nonlinearities introduced by end stops and control strategies, the mathematical model occasionally becomes very stiff. A variable step solver, MATLAB's ode23tb algorithm, has therefore been used for the numerical integration of the model (3). The relative tolerance was set to 10^{-4}, and the absolute tolerance to 10^{-3} for most of the simulations.

In order to study adaptive parameter tuning, we also define a set of cases where the sea state changes gradually. This is done by adding time series for two different sea states, where each series is weighted such that the resulting time series is changing linearly with time from one to the other:

$$F_e(t) = F_{e,1}(t)\left(1 - \frac{t}{T_f}\right) + F_{e,2}(t)\frac{t}{T_f} \tag{19}$$

where T_f=43.2 ks (12 h) is the length of the time series. For the results to be presented here, $F_{e,1}$ was synthesized from a Bretschneider spectrum with parameters T_e=6 s and H_s =1.41 m, and $F_{e,2}$ correspondingly with parameters T_e=12 s and H_s=2.83 m.

5 Results and Discussion

In this section, the results are presented in three parts. First, we look at regular wave results, which indicate some basic properties of the different controllers. We then turn to the irregular wave results where the real potential of different strategies may be revealed. Finally, some examples of adaptive control are given with the use of gain scheduling and extremum-seeking control in a changing sea state.

5.1 Regular Waves. A Budal diagram [43] giving the absorbed power as a function of wave height is shown in Fig. 20. Because the waves are regular, the simulations have been run using ideal prediction (i.e., the future is assumed known). Most of the control strategies are able to give close to optimal absorption in the low-period range. The exceptions are the RL and ATV control strategies. For resistive loading, the reason for the discrepancy is the phase deviation between excitation force and velocity. On the other hand, the reason why the AVT control, which gives perfect phase, fails to reach optimum for low periods is that the amplitude is nonoptimal. For this strategy all the wave periods have been run with the same value $1/\{2R_c\}$ for the force-to-velocity feed-forward function, where R_c was set equal to $R_i(\omega_k)$ with ω_k=$2\pi/(9\ \text{s})$=0.70 rad/s. It means that unconstrained oscillations will have the right phase but the amplitude will only be correct for T=$2\pi/\omega_k$=9 s. This may be seen from the curve, which shows good absorption for wave periods in the range 8–10 s. The force-to-velocity feed-forward function was defined as a constant in order to see the effect of varying wave period. If we had instead optimized its value at each wave period, the result would be similar to ACC control.

The amplitude restriction causes the absorption curves to eventually depart from the theoretical ascending limit included in Fig. 20. We observe that, for long wave periods, the MPC controller performs better than the other strategies, and this is because it is able to account for the amplitude restriction in an optimal way. The difference between ACC and latching/clutching algorithms is somewhat more complex. For low wave height the ACC controller performs better because it supplies reactive power so that the optimum amplitude may be achieved where the natural "unaided" amplitude response would be too low. For larger wave heights, this is not needed, and the time-variant latching and clutching strategies are able to yield a larger absorbed power, as seen in Fig. 21. Their oscillation pattern is beneficial in comparison to the linear time-invariant (sinusoidal) response we get with ACC control. As shown by Budal et al. [36], an explanation for this is that with latching control, the amplitude of the first harmonic component of the position response has a larger amplitude than the physical amplitude (which has here been restricted to 3 m). This also applies to the MPC time series in Fig. 13, which is the constrained optimal solution [9]. It resembles a latching control response. As we can see, the result is that the PML algorithm gives higher absorbed power than ACC for high wave amplitudes (due to the amplitude restriction), which has also been reported before [34].

As mentioned before, in regular waves, the threshold unlatching (TUL) and unclutching (TUC) strategies become identical to the corresponding peak-matching counterparts (PML and PMC, respectively). This is the reason why they are not included in Figs. 20 and 21.

An important issue, which should be given thorough consideration for wave energy appliances, is the peak-to-average power ratio [34]. For the reactive control algorithms (ACC, AVT, and MPC), it is shown in Fig. 22. For the RL strategy, this ratio is always equal to two in regular waves because the instantaneous absorbed power is oscillating harmonically about the average absorbed power $\bar{P}_a$ with frequency twice the wave frequency and with amplitude $\bar{P}_a$. We see that the MPC strategy requires higher

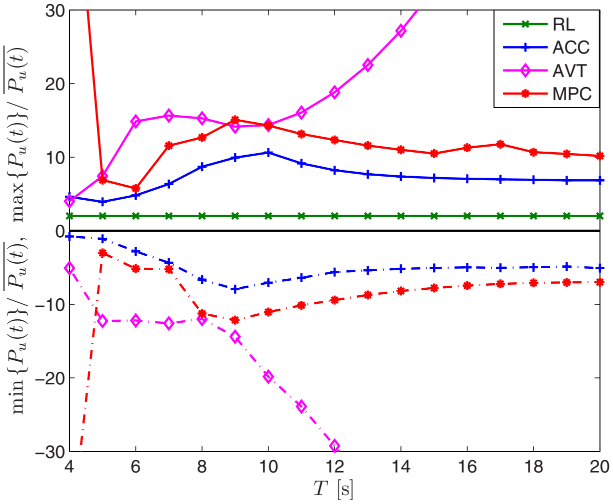

Fig. 22 Peak-to-average ratio for the absorbed power in regular waves with height 1 m for the controllers giving reactive power flow

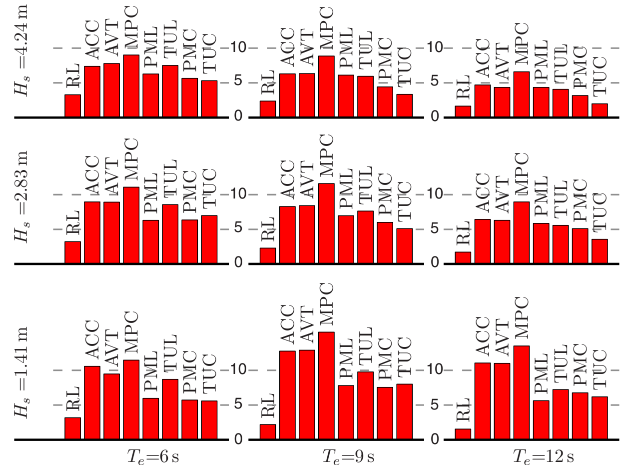

Fig. 24 Absorption width $d_a = \bar{P}_u / J$ (m) (based on absorbed useful energy) for the simulation in irregular waves and different control strategies. Horizontal dashed lines are drawn at d_a =5 m and d_a=10 m. The sea states were synthesized from a Bretschneider spectrum, and significant wave height and energy period are given to the left and on the bottom of the graph, respectively. The wave power level for each sea state may be read from Table 1.

instantaneous power than the ACC controller. With these controllers, the maximum inverted power (i.e., machinery working as a motor) is almost as large as the maximum converted power.

The large peak-to-average power ratios for the AVT strategy is due to the low average values—for the range of periods where the absorbed power is close to optimum (8–9 s), the peak to-average ratio is close to the MPC result.

The corresponding data for the latching and clutching control strategies are given in Fig. 23. These two strategies give no reactive power flow (and thus no power inversion) and have similar levels of average absorbed power. The curves reveal a very interesting trend: whereas the ratio for latching control is increasing almost linearly with T, the clutching control gives a decreasing peak-to-average ratio as the wave period increases. This is easy to understand: As the period increases, the transition intervals (where the latching algorithm extracts power) become shorter and shorter relative to the intervals of high resistance (where the clutching algorithm extracts power). The clutching strategy eventually even gives a lower ratio than the RL strategy. In general, the latching and clutching controllers have smaller peak-to-average power ratios than the reactive controllers ACC, AVT, and MPC.

5.2 Irregular Waves. For the simulations with irregular wave time series, the controllers are run as if they were operating in real

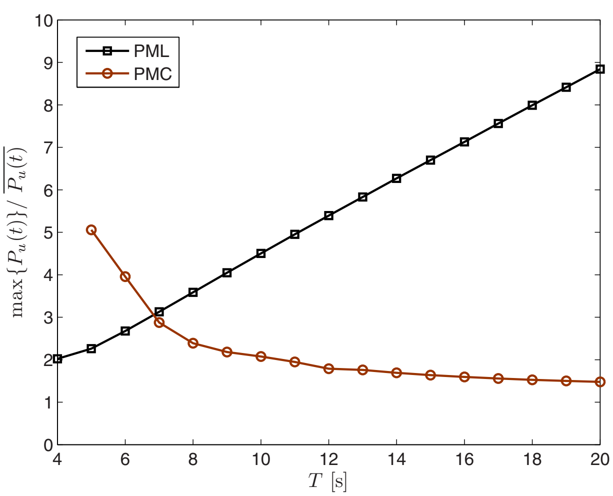

Fig. 23 Peak-to-average power ratio in regular waves with height 1 m for the controllers without reactive power flow

time with access to accurate estimates of the system states and the instantaneous excitation force F_e. The MPC and peak-matching controllers need knowledge of F_e ahead, and these and augmented Kalman filter have been used for prediction, identical to the one used in Ref. [9]. In practice, forecasts may be obtained from a pressure transducer measuring the hydrodynamic pressure close to the buoy by using an estimator to derive an estimate for the excitation force from this measurement. For the peak-matching strategies a prediction equal to $T_0/4 \approx 1.1$ s has been used, and for the MPC strategy the prediction horizon was equal to 2.2 s.

In each case the control parameters, including the ATV feed-forward constant, have been optimized to yield the maximum average absorbed power over the irregular wave time series. The optimization was done with a simplex algorithm (MATLAB's *fminsearch* function [41]).

Figure 24 shows the resulting numbers for the average absorbed power. There is a significant gain in power for all controllers compared with the RL case (which has also been optimized for each sea state). As expected, the MPC controller gives the superior performance in terms of converted power. Overall, the ACC strategy is the second best in terms of absorbed power, with a reduction in the range 10–25% compared with the MPC algorithm. The ACC control always gives higher absorbed useful power than the AVT control the way we have implemented them, but in some cases only slightly. Because the AVT feed-forward constant has been optimized for each sea state, the drastic performance reduction for large wave periods in regular waves (see Fig. 20) has been avoided.

In the sea states of smaller waves, the latching and clutching strategies, which give similar results, are significantly weaker than the reactive control algorithms, but this gap is reduced or even vanishing when the wave heights become high enough. A corresponding effect would thus be expected if the buoy was reduced in size and run in the same sea state.

It may be surprising to see that the threshold unlatching and unclutching strategies in some cases give more power than the peak-matching strategies. This, however, is due to inaccurate predictions. Runs with ideal prediction (future assumed known) in irregular waves showed that then the peak matching always gives an absorbed power higher than or equal to the threshold strategies. It is also a general trend that the threshold unlatching strategy (TUL) gives a somewhat higher converted power than the corre-

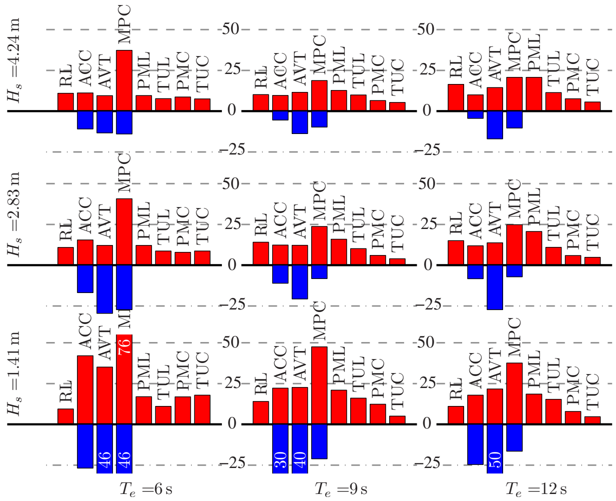

Fig. 25 Peak-to-average ratio for the power flowing through the machinery for incident irregular waves. The wave excitation corresponds to the results presented in Fig. 24. Horizontal dashed lines are drawn at the values −25, 25, and 50. Some of the bars go outside the scale. Their sizes are then given by the white numbers.

sponding clutching strategy (TUC). It should be mentioned that the clutching gives higher power dissipation in the end stops than the other control methods. If this energy can be converted to useful energy, our data show that the difference between clutching and latching algorithms would be reduced, but not canceled.

In general it is seen that the absorption width is decreasing with increasing wave amplitudes/heights. This is due to increasing influence from the amplitude restriction as the wave height increases.

Turning now to the peak-to-average ratios in Fig. 25, an important observation is the large instantaneous power flow required by the MPC, especially for low wave periods, where the ratios exceed 25 for the reactive power controllers. High peak-to-average ratios will probably be a strong cost driver for most types of machinery, and it is therefore crucial to find machinery and controller designs that can meet this challenge.

The ACC strategy has negative ratios (motor mode) comparable to the MPC controller, whereas the positive ratios (generator mode) are considerably lower. This is interesting because the reduction in converted power is in most cases modest. The ACC strategy may therefore occur as an attractive alternative to MPC when trade-offs between power output and peak-to-average ratios have to be made in the design of machinery and controller.

On the other hand, a large advantage with MPC control is the flexibility for including constraints. For a real machinery, force constraints could be set such that these excessive peak-to-average ratios would have been reduced, of course with a due reduction in absorbed power. The large negative power peaks observed for the AVT strategy are due to large accelerations demanded by the controller when the velocity reference is returning to the valid area of the phase plane after having been outside (Fig. 19). These can probably be mitigated by including additional constraints on the velocity reference signal.

However, the most encouraging observation is perhaps the low ratios found for the clutching strategies, as was also observed for regular waves. This fact, together with the absence of reactive power flow, leads to a conclusion that clutching would be a very interesting alternative if it can be implemented with a viable machinery design. For the sea states used here, the latching control algorithms give positive peak-to-average ratios comparable to the ACC and AVT controllers, except for the case of small waves and small wave periods, where the ratios are smaller.

Between latching and clutching strategies, the threshold strategies give lower peak-to average ratios than the peak-matching algorithms. It is also worth noticing that in the direction of large amplitudes and large wave periods, the primitive RL strategy eventually gives higher peak-to-average ratios than the high-yield ACC and AVT strategies. For the ACC controller the need for reactive power mainly depends on wave period (and not wave height) once the amplitude constraint is reached [34], and because the average absorbed power increases for increasing wave heights, the peak-to-average therefore decreases monotonically with increasing wave height. For the RL strategy it is quite constant compared with the other strategies.

Table 2 gives a schematic summary of the properties and performance observed for the strategies that have been investigated.

5.3 Adaptive Control. Examples of automatic parameter tuning are shown in Figs. 26 and 27. From the curves of accumulated energy it is verified that the tuning gives an increased energy yield as compared with the constant parameter case for all the shown strategies (RL, ACC, and TUL). It may also be observed that the gain scheduling strategy partly gives a parameter variation similar to the extremum-seeking strategy, only slightly delayed. We interpret the delay to be due to the computation of average values, which are based on analysis of the last 100 wave up-crossing periods. The effect of the parameter tuning is largest for the RL and ACC strategies. The TUL controller is only weakly sensitive to changes in the threshold setting. Toward the end of the time series for ACC control (Fig. 27(*b*)) runs with constant parameter give very poor results for the absorbed power, which even decays toward the end. This is due to heavy power dissipation in the end stops instead of conversion to useful power. The gain scheduling strategy is not able to capture the effect of constrained amplitudes

Table 2 Comparison of properties and performance for the investigated control strategies. The second and third columns give the feedback (FB) route, while the fourth column indicates the need for feeding forward an estimate of the excitation force. The column with relative average power gives values in percentage compared with the power converted using the MPC algorithm. The last column gives the mean peak-to-average ratio. All numbers are found as an average over the 9 sea states that were simulated, see Table 1 and Figs. 24 and 25.

Method	Direct velocity FB	Velocity tracking	F_e feed forward	F_e prediction needed	Constrained optimal	Reactive power flow	Nonlinear F_m	Relative average power	Mean peak-to-average
RL	x							23	12
ACC	x					x		78	17
AVT		x	x			x		77	17
MPC		x	x	x	x	x	x	100	36
PML	x		x	x			x	59	18
TUL	x		x				x	68	11
PMC	x		x	x			x	53	9
TUC	x		x				x	47	6

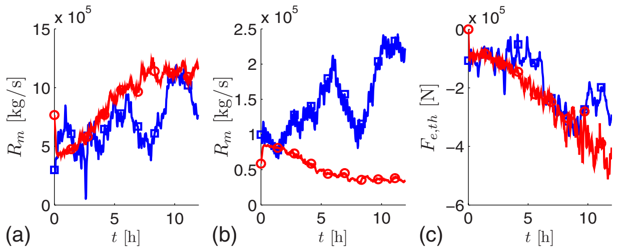

Fig. 26 Control parameter values for the three of the control strategies with automatic tuning. The red circle-marked curves result from parameter tuning by gain scheduling, and the blue square-marked curves are due to extremum-seeking control. The sea state is a weighted sum (see Eq. (19)) of two sea states, one with T_e=6 s and H_s=1.41 m and the other with T_e=12 s and H_s=2.83 m.

as the parameter setting only depends on the wave period. This is the reason why the extremum-seeking strategy performs better for ACC and TUL control when the sea changes to a state with high power level (T_e=12 s and H_s=2.83 m). This could be compensated for by finding a parameter mapping where the gain scheduling also depends on the wave amplitude. However, this has not been done herein.

The simulation work has shown that we could not manage to tune/optimize the control parameters on a shorter time scale than corresponding to sea state average (about 15–30 min intervals). Thus only the MPC control, which works on a wave-to-wave time scale, is able to approach the theoretical optimum when the motion is constrained.

6 Conclusion

A selection of strategies for real-time control of wave energy converters has been defined and applied to the example of a heaving-buoy wave absorber. The strategies include velocity proportional and approximate complex conjugate control, PI-controlled tracking of the approximate optimum velocity, latching and clutching algorithms, as well as a model-predictive controller. The controller aim has been to maximize the power output from the converter in a set of sea states representative for irregular deep-water waves. The controllers were provided with different means to handle amplitude constraints, and were run for irregular waves without assuming any a priori knowledge of the forces from the incident waves.

It was found that real-time extremum-seeking control and gain scheduling using short-time historical wave data both are promising methods for parameter tuning in these controllers for wave energy conversion. In irregular waves, improved power conversion was achieved with both methods as compared with running with constant control parameters in a simple test case.

Constraints on the motion amplitude were implemented as spring and damper elements for most of the control algorithms

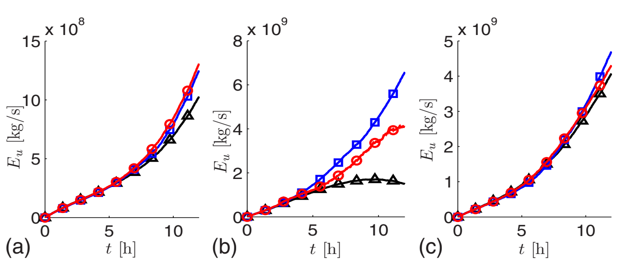

Fig. 27 Accumulated useful energy corresponding to the cases presented in Fig. 26. The black triangle-marked curve gives the energy absorbed without parameter tuning (i.e., keeping the initial setting throughout the simulation).

investigated. For the velocity tracking controller, a phase-plane constraint was implemented, which worked well in avoiding impact with the end stop mechanism.

It was found that a common challenge for several of the controllers is the large reactive power through the machinery needed in order to supply the computed machinery force. This means that the machinery must be designed for a much larger instantaneous power than the average power that the converter is able to deliver. This is an important challenge to the design of machinery systems for wave energy converters. If the intention is to apply reactive control, the system should be designed with an energy storage as early as possible in the conversion chain such that only the upstream part has to be designed to support the large reactive power.

Although simple, the latching and clutching strategies have several properties that make them attractive despite the fact that their performance in terms of absorbed power is inferior to the best performing controllers in this study. They may be very easy to implement and ideally do not require any reactive power flow through the machinery. Compared with the MPC controller, the absorbed useful power is in the range of about 40–80%, but the peak-to-average power ratio is typically about 20–50% for the latching control and 20–30% for the clutching control. In the constrained case (relatively high waves), the peak-to-average ratio is comparable to approximate complex conjugate and optimal velocity control for the latching control strategy. Interestingly, the lowest ratios are found for clutching control, where the ratios are, in fact, usually lower than for pure resistive loading.

Acknowledgment

The authors would like to thank the Norwegian Research Council for financial support through the Centre for Ships and Ocean Structures (CeSOS). Special thanks go to Professor Thor Inge Fossen for fruitful discussions in connection with this work.

Nomenclature and Abbreviations

β = filter frequency ratio [1]
η = heave position (m)
ω = angular frequency (rad/s)
ρ = ocean water density (1025 kg/m^3)
A = area (m^2)
$\mathbf{A}$ = state-space system matrix
$\mathbf{B}$ = state-space input matrix
$\mathbf{C}$ = state-space output matrix
ACC = approximate complex conjugate (control)
AVT = approximate optimal velocity tracking
F = force (N)
FB = feedback
H = transfer function
H = wave height (m)
H_s = significant wave height (m)
MPC = model-predictive control
K = controller gain
P = power (W)
R = resistance (kg/s)
RL = resistive loading
S = hydrostatic stiffness in heave (N/m)
T = period (s)
T_e = energy period (s)
X = reactance (kg/s)
Z = impedance (kg/s)
g = acceleration of gravity (9.81 m/s^2)
k = retardation function the radiation force (kg/s)
m = mass (kg)
m_r = added mass (kg)
s = Laplace variable (s^{-1})
$\mathrm{sign}(\cdot)$ = signum function
t = time (s)

$u(\cdot)$ = Heaviside step function
v = velocity (m/s)
x = element of $\mathbf{x}$
$\mathbf{x}$ = state-space vector
$\mathbf{z}$ = radiation model state vector

Subscripts

HP = high-pass
I = integral
LP = low-pass
P = proportional
R = radiation (total)
a = absorbed
c = constant
e = excitation
es = end stop
f = final
i = intrinsic
i = inertia
k = index
l = latching
lim = limit
m = machinery
max = maximum
h = horizon
r = radiation
ref = reference
s = stiffness
u = system/plant
u = useful
v = velocity
w = water plane
0 = relating to resonance
∞ = regarding $\omega \rightarrow \infty$
$a \times b$ = dimensions, vertical $\times$ horizontal

Superscripts

opt = optimal
* = complex conjugate
$^-$ = mean value

References

[1] Evans, D. V., 1981, "Power From Water Waves," Annu. Rev. Fluid Mech., **13**, pp. 157–187.
[2] Falnes, J., 2002, "Optimum Control of Oscillation of Wave-Energy Converters," Int. J. Offshore Polar Eng., **12**(2), pp. 147–155.
[3] Falnes, J., 2002, *Ocean Waves and Oscillating Systems: Linear Interactions Including Wave-Energy Extraction*, Cambridge University Press, Cambridge.
[4] Price, A. A. E., Forehand, D. I. M., and Wallace, A. R., 2009, "Time-Span of Future Information Necessary for Theoretical Acausal Optimal Control of Wave Energy Converters," Proceedings of the European Control Conference 2009, Budapest, Hungary, pp. 3761–3766.
[5] Perdigão, J. N. B. A., and Sarmento, A. J. N. A., 1989, "A Phase Control Strategy for OWC Devices in Irregular Seas," The Fourth International Workshop on Water Waves and Floating Bodies, J. Grue, ed., Department of Mathematics, University of Oslo, pp. 205–209.
[6] Beirão, P. J. B. F. N., 2007, "Modelling and Control of a Wave Energy Converter: Archimedes Wave Swing," Ph.D. thesis, Universidade Tecnica de Lisboa, Delft.
[7] Gieske, P., 2007, "Model Predictive Control of a Wave Energy Converter: Archimedes Wave Swing," MS thesis, Delft University of Technology, Delft.
[8] Eidsmoen, H., 1995, "On the Theory and Simulation of Heaving-Buoy Wave-Energy Converters With Control," Ph.D. thesis, NTH (now NTNU), Trondheim.
[9] Hals, J., Falnes, J., and Moan, T., 2011, "Constrained Optimal Control of a Heaving Buoy Wave-Energy Converter," ASME J. Offshore Mech. Arct. Eng., **133**(1), p. 011401.
[10] Kamenský, M., and Guglielmi, M., 2007, "Optimal Control of Power Take-Off From Mass Spring-Damper System," 16th International on Process Control 2007.
[11] Nolan, G., Ringwood, J., Leithead, W., and Butler, S., 2005, "Optimal Damping Profiles for a Heaving Buoy Wave Energy Converter," Proceedings of the 15th International Offshore and Polar Engineering Conference, ISOPE, Seoul, Korea.
[12] Hoskin, R. E., and Nichols, N. K., 1987, "Optimal Strategies For Phase Control Of Wave Energy Devices," in *Utilization of Ocean Waves—Wave to Energy Conversion*, M. E. McCormick and Y. C. Kim, ed., American Society of Civil Engineering, New York, pp. 184–199.
[13] Naidu, D. S., 2003, *Optimal Control Systems*, CRC, Boca Raton, FL.
[14] Budal, K., and Falnes, J., 1980, "Interacting Point Absorbers With Controlled Motion," Power from Sea Waves, B. Count, ed., Academic, London, pp. 381–399.
[15] Budal, K., Falnes, J., Iversen, L. C., Lillebekken, P. M., Oltedal, G., Hals, T., Onshus, T., and Høy, A. S., 1982, "The Norwegian Wave-Power Buoy Project," Proceedings of the Second International Symposium on Wave Energy Utilization, H. Berge, ed., Tapir, Trondheim, Norway, pp. 323–344.
[16] Babarit, A., 2005, "Optimisation hydrodynamique et contrôle optimal d'un récupérateur de l'énergie des vagues," Ph.D. thesis, Ecole Centrale de Nantes, Nantes.
[17] Hals, J., Taghipour, R., and Moan, T., 2007, "Dynamics of a Force-Compensated Two Body Wave Energy Converter in Heave With Hydraulic Power Take-Off Subject to Phase Control," Proceedings of the 7th European Wave and Tidal Energy Conference, Porto, Portugal.
[18] Falnes, J., 1999, "Wave-Energy Conversion Through Relative Motion Between Two Single Mode Oscillating Bodies," ASME J. Offshore Mech. Arct. Eng., **121**, pp. 32–38.
[19] Falcão, A. F. O., 2007, "Phase Control Through Load Control of Oscillating-Body Wave Energy Converters With Hydraulic PTO System," Proceedings of the Seventh European Wave and Tidal Energy Conference, Porto, Portugal.
[20] Lopes, M., Hals, J., Gomes, R., Moan, T., Gato, L., and Falcao, A. O., 2009, "Experimental and Numerical Investigation of Non-Predictive Phase-Control Strategies for a Point-Absorbing Wave Energy Converter," Ocean Eng., **36**(5), pp. 386–402.
[21] Salter, S. H., Taylor, J. R. M., and Caldwell, N. J., 2002, "Power Conversion Mechanisms for Wave Energy," Proceedings of Institute of Mechanical Engineers, Part M, Engineering for the Maritime Environment, **216**, pp. 1–27.
[22] Babarit, A., Guglielmi, M., and Clement, A. H., 2009, "Declutching Control of a Wave Energy Converter," Ocean Eng., **36**(12–13), pp. 1015–1024.
[23] Evans, D. V., 1981, "Maximum Wave-Power Absorption Under Motion Constraints," Appl. Ocean. Res., **3**(4), pp. 200–203.
[24] Pizer, D., 1993, "Maximum Wave-Power Absorption of Point-Absorbers Under Motion Constraints," Appl. Ocean. Res., **15**(4), pp. 227–234.
[25] Falnes, J., 2000, "Maximum Wave-Energy Absorption by Oscillating Systems Consisting of Bodie and Water Columns With Restricted or Unrestricted Amplitudes," Proceedings of the International Offshore and Polar Engineering Conference, Vol. 1, pp. 420–426.
[26] Leijon, M., Danielsson, O., Eriksson, M., Thorburn, K., Bernhoff, H., Isberg, J., Sundberg, J., Ivanova, I., Sjöstedt, E., Agren, O., Karlsson, K., and Wolfbrandt, A., 2006, "An Electrical Approach to Wave Energy Conversion," Renewable Energy, **31**(9), pp. 1309–1319.
[27] de Sousa Prado, M., Gardner, F., Damen, M., and Polinder, H., 2006, "Modelling and Test Results of the Archimedes Wave Swing," Proc. Inst. Mech. Eng., Part A, **220**(8), pp. 855–868.
[28] Brown, R. G., and Hwang, P. Y. C., 1997, *Introduction to Random Signals and Applied Kalman Filtering*, 3rd ed., Wiley, New York.
[29] Astrom, K. J., and Wittenmark, B., 2008, *Adaptive Control*, Dover, New York.
[30] Ariyur, K. B., and Krstic, M., 2003, *Real-Time Optimization by Extremum-Seeking Control*, Wiley, New York.
[31] Cummins, W. E., 1962, "The Impulse Response Function and Ship Motions," Schiffstechnik, **9**, pp. 101–109.
[32] Jefferys, E. R., 1984, "Simulation of Wave Power Devices," Appl. Ocean. Res., **6**(1), pp. 31–39.
[33] Taghipour, R., Perez, T., and Moan, T., 2008, "Hybrid Frequency-Time Domain Models for Dynamic Response Analysis of Marine Structures," Ocean Eng., **35**(7), pp. 685–705.
[34] Hals, J., Bjarte-Larsson, T., and Falnes, J., 2002, "Optimum Reactive Control and Control by Latching of a Wave-Absorbing Semisubmerged Heaving Sphere," Proceedings of the International Conference on Offshore Mechanics and Arctic Engineering—OMAE, Vol. 4, pp. 415–423.
[35] Nebel, P., 1992, "Maximizing the Efficiency of Wave-Energy Plants Using Complex Conjugate Control," Proceedings of the Institution of Mechanical Engineers. Part I Journal of Systems and Control Engineering, **206**(4), pp. 225–236.
[36] Budal, K., Falnes, J., Hals, T., Iversen, L. C., and Onshus, T., 1981, "Model Experiment with a Phase Controlled Point Absorber," Proceedings of the Second International Symposium on Wave and Tidal Energy, H. S. Stephens and C. A. Stapleton, eds., BHRA Fluid Engineering (Cranford, Bedford), Cambridge, UK, pp. 191–206.
[37] Babarit, A., Duclos, G., and Clement, A. H., 2004, "Comparison of Latching Control Strategies for a Heaving Wave Energy Device in Random Sea," Appl. Ocean. Res., **26**(5), pp. 227–238.
[38] Killingsworth, N., and Krstic, M., 2005, "Auto-Tuning of PID Controllers via Extremum Seeking," Proceedings of the American Control Conference, Vol. 4, pp. 2251–2256.
[39] Spong, M. W., 2006, *Robot Modeling and Control*, Wiley, Hoboken, NJ.
[40] Edwards, C., and Spurgeon, S. K., 1998, *Sliding Mode Control*, CRC, Boca Raton, FL.
[41] The Mathworks Inc., 2006, MATLAB, version 7.2, URL: http://www.mathworks.com/
[42] WAMIT, 2006, WAMIT User Manual, version 6.3, http://www.wamit.com
[43] Falnes, J., 2007, "A Review of Wave-Energy Extraction," Mar. Struct., **20**(4), pp. 185–201.